Supplementary Material

Trans-dural cerebrospinal fluid efflux to skull bone marrow in humans with CSF disorders

Geir Ringstad[1], Per Kristian Eide[2,3]

[1]Dept. of Radiology, Oslo University Hospital - Rikshospitalet, Norway

[2]Dept. of Neurosurgery, Oslo University Hospital-Rikshospitalet, Norway,

[3]Institute of Clinical Medicine, Faculty of Medicine, University of Oslo, Oslo, Norway

Correspondence:

Professor Per Kristian Eide, MD PhD

Department of Neurosurgery

Oslo University Hospital - Rikshospitalet

Pb 4950 Nydalen,

N-0424 Oslo, Norway

p.k.eide@medisin.uio.no

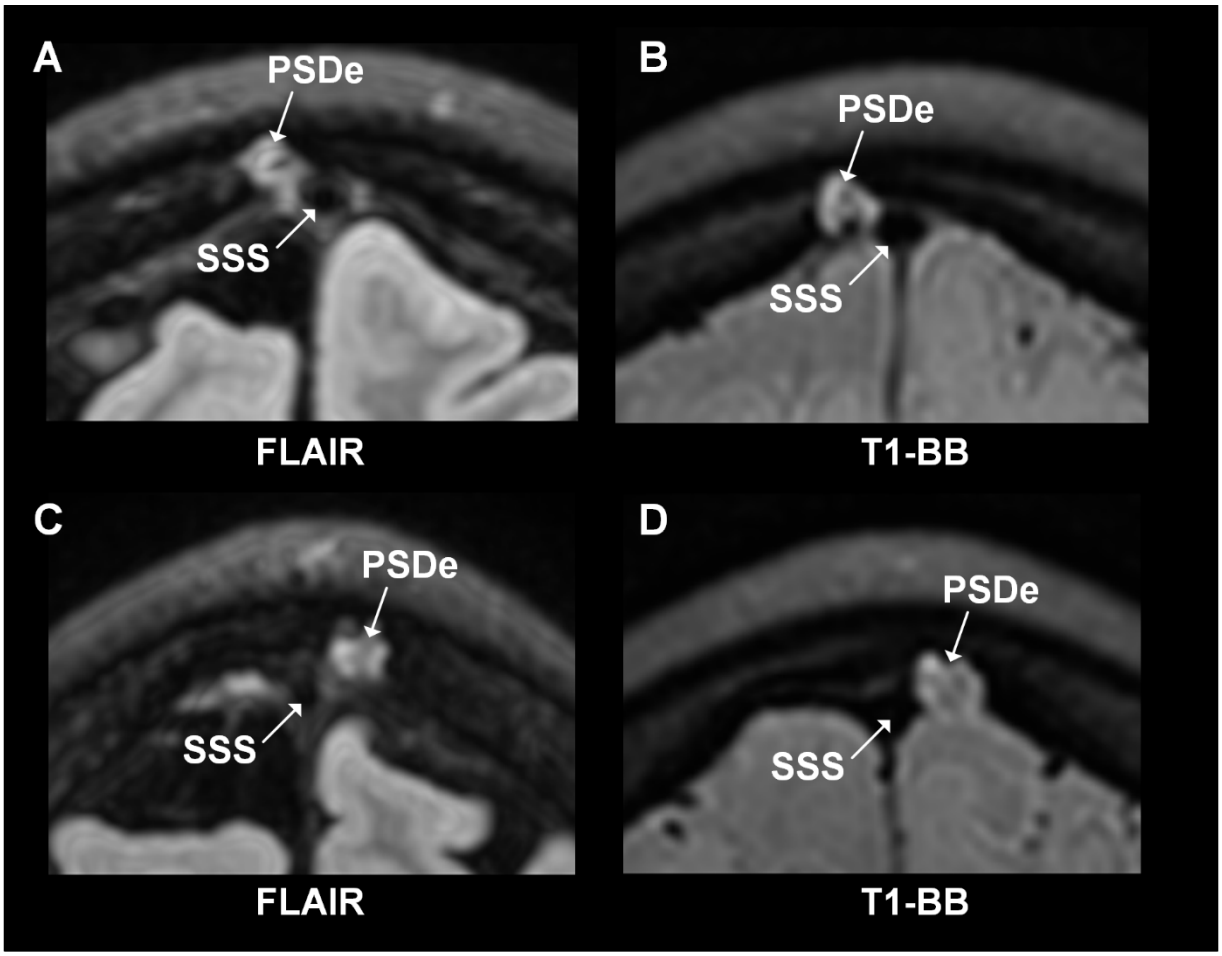

Suppl. Fig. 1. FLAIR versus T1-BB images (coronal sections at skull vertex). FLAIR images (left column) were used to identify PSD, PSDe and De, while pre-contrast T1-BB images (right column) were used to rule out macroscopic elements of venous flow within PSD and to measure signal change over time (Fig. 4 and Suppl Fig. 11). Images (**A**)-(**B**) are from the same individual, as are images (**C**)-(**D**). De: Dural extensions to skull bone marrow in distance from parasagittal dura. PSD: Parasagittal dura. PSDe: Parasagittal dura extensions to skull bone marrow. SSS: Superior sagittal sinus.

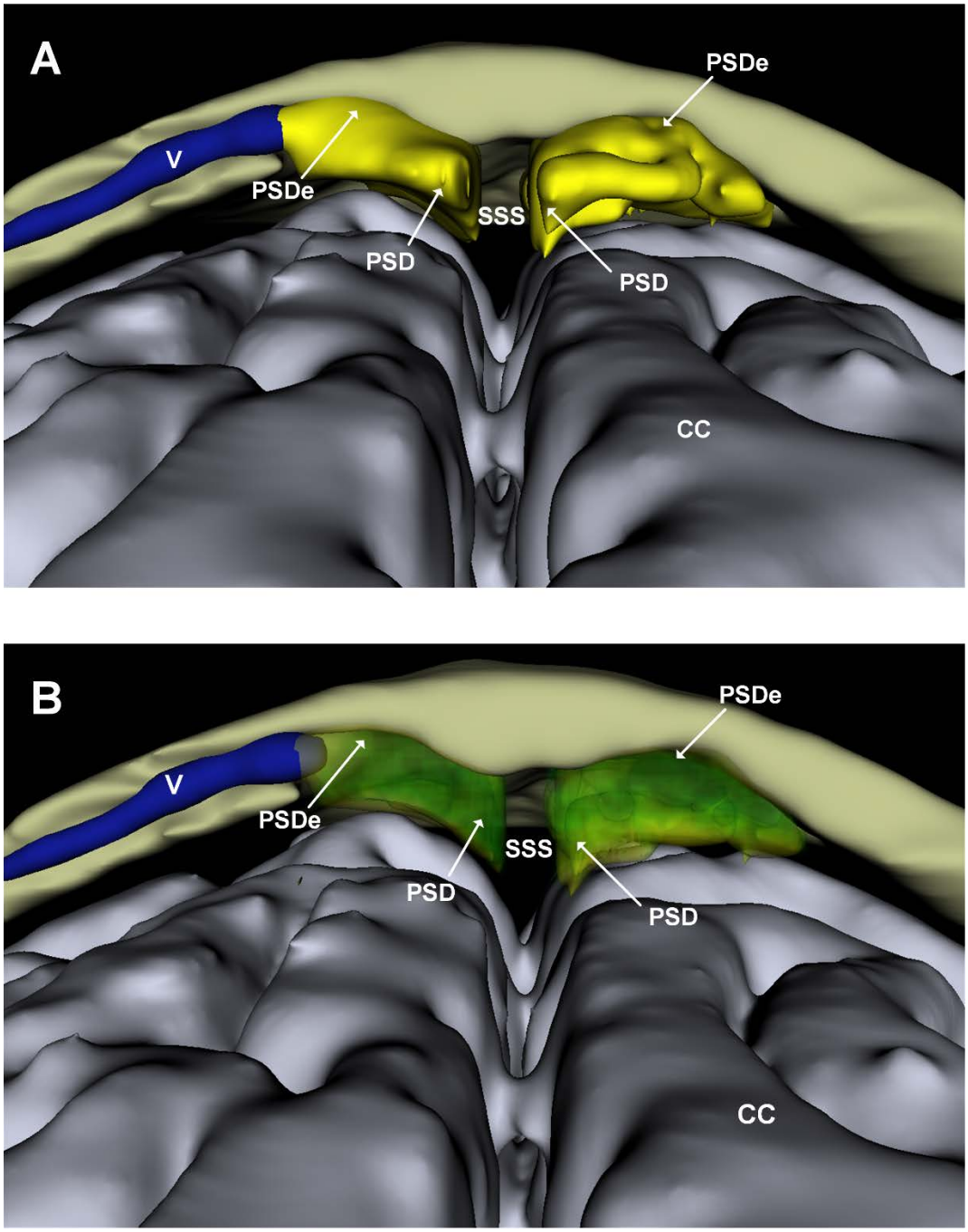

Suppl. Fig. 2. 3D presentation of tracer enrichment within parasagittal dura (coronal section at skull vertex). In (**A**) is shown the surface of the cerebral cortex (CC; grey), and the intradiploic parasagittal dural extension (PSDe; yellow) adjacent to superior sagittal sinus (SSS) prior to intrathecal tracer. An intradiploic vein (V, dark blue) is shown nearby the parasagittal dura and located within the intradiploic skull space (beige) where skull bone marrow is located. In (**B**) the parasagittal dura (PSD) and PSDe (green) has become enriched by the tracer administered intrathecally. The cerebrospinal fluid in the subarachnoid space is subtracted from the images. Images: Tomas Sakinis, MD.

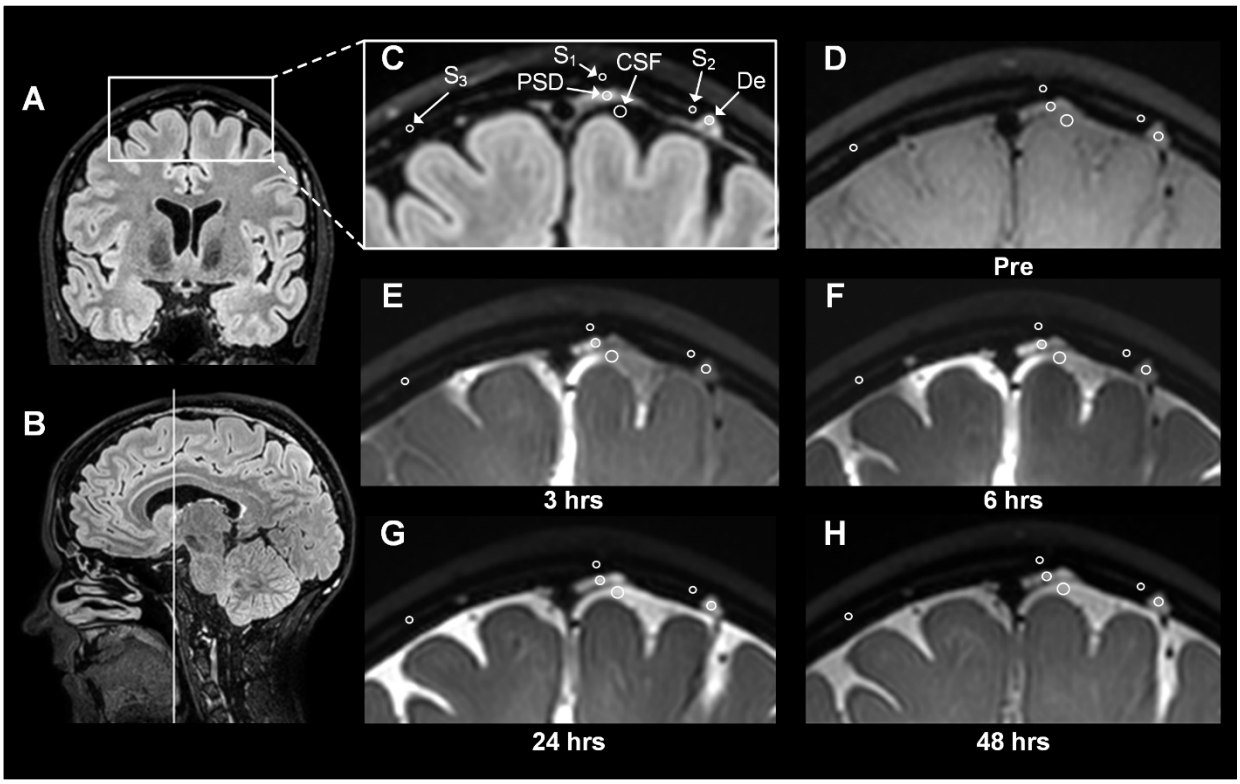

Supp. Fig. 3. Placement of regions of interest (ROIs). For identification of anatomical structures, we used the T2-FLAIR images (**A**-**C**). Regions of interest (ROIs) within the cerebrospinal fluid (CSF) were placed nearby parasagittal dura (PSD), or nearby the dura extensions (De) into diploe in distances from PSD. The intradural compartments included PSD, parasagittal dura extensions (PSDe) into diploic area, and dura extensions (De) into diploe in distance from PSD. The ROIs within diploe of skull bone marrow were either nearby PSD or PSDe (S_1), nearby the De (S_2), or in distance (remote) from visible dura extensions into diploe (S_3). Utilizing T1-BB sequences, areas with blood flow could be ruled out and enrichment of tracer within the different locations were semi-quantified by placing the ROIs within exactly the same locations at each time point. The size of each ROI was adjusted to avoid partial volume averaging. Examples of placement of ROIs using T1-BB are presented for images before (Pre; **D**), and after 3 (**E**), 6 (**F**), 24 (**G**) and 48 (**H**) hours.

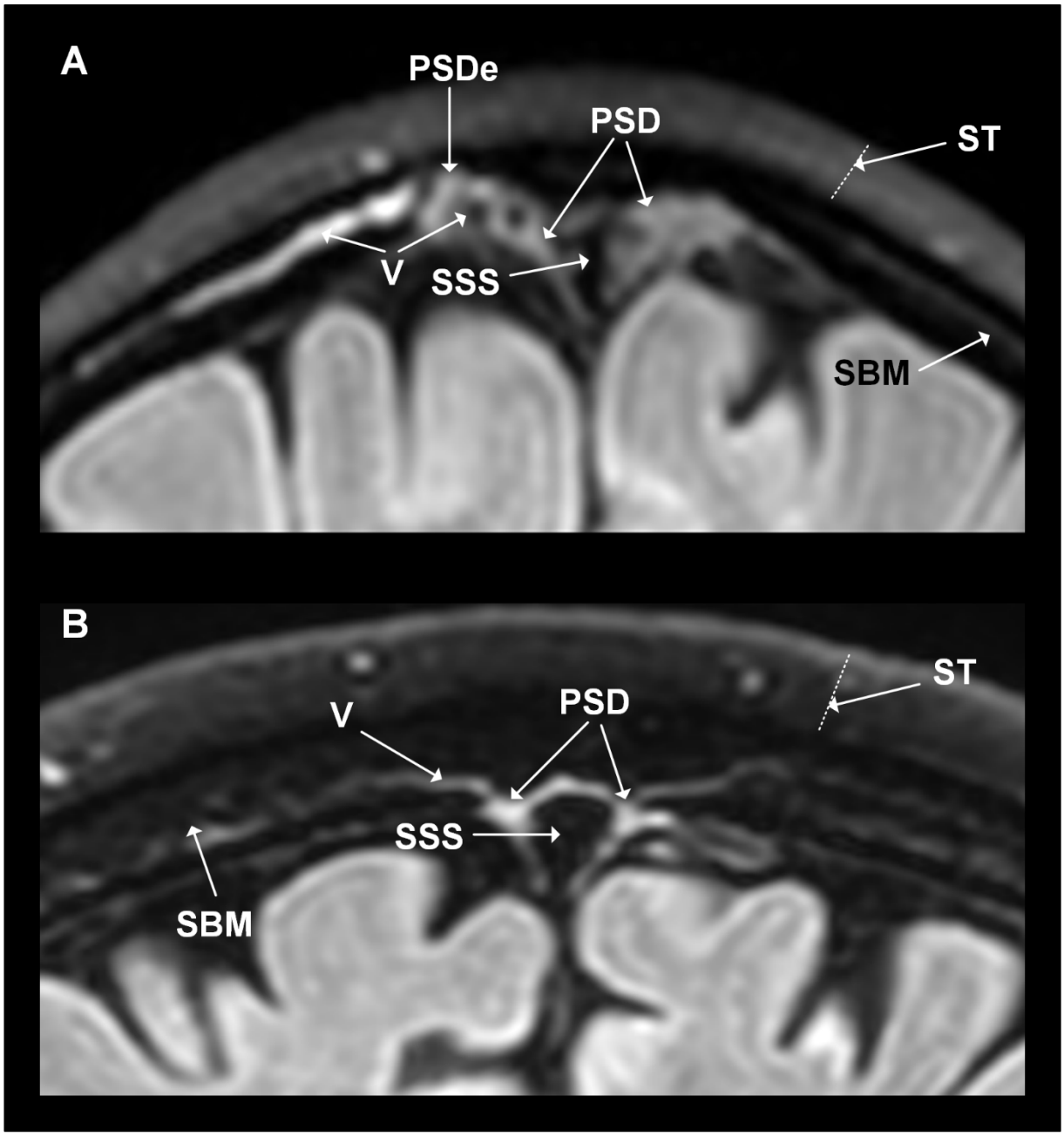

Suppl. Fig 4. Variation in size of parasagittal dura (coronal sections at skull vertex). There is substantial inter-individual variation in size of parasagittal dura (PSD) in humans, here illustrated by T2-FLAIR images in (**A**) a 28 years old reference subject examined for chronic headache and (**B**) a 51 years old individual with headache and cognitive impairment, and a diagnosis of fronto-temporal dementia. It may be noted that the PSD/PSDe in (a) has a much larger volume than the PSD in (b). Both images show veins within skull bone marrow (SBM) to be continuous with PSD. In (a), it may also be noted veins (V) of cerebral drainage traversing the PSD before entry into SSS. Veins (V) with dark signal at T2-FLAIR reflect signal loss from blood flow, and with higher velocity than in intradiploic veins, where signal suppression does not occur due to slow flow velocity. SSS: Superior sagittal sinus. ST: Superficial tissue.

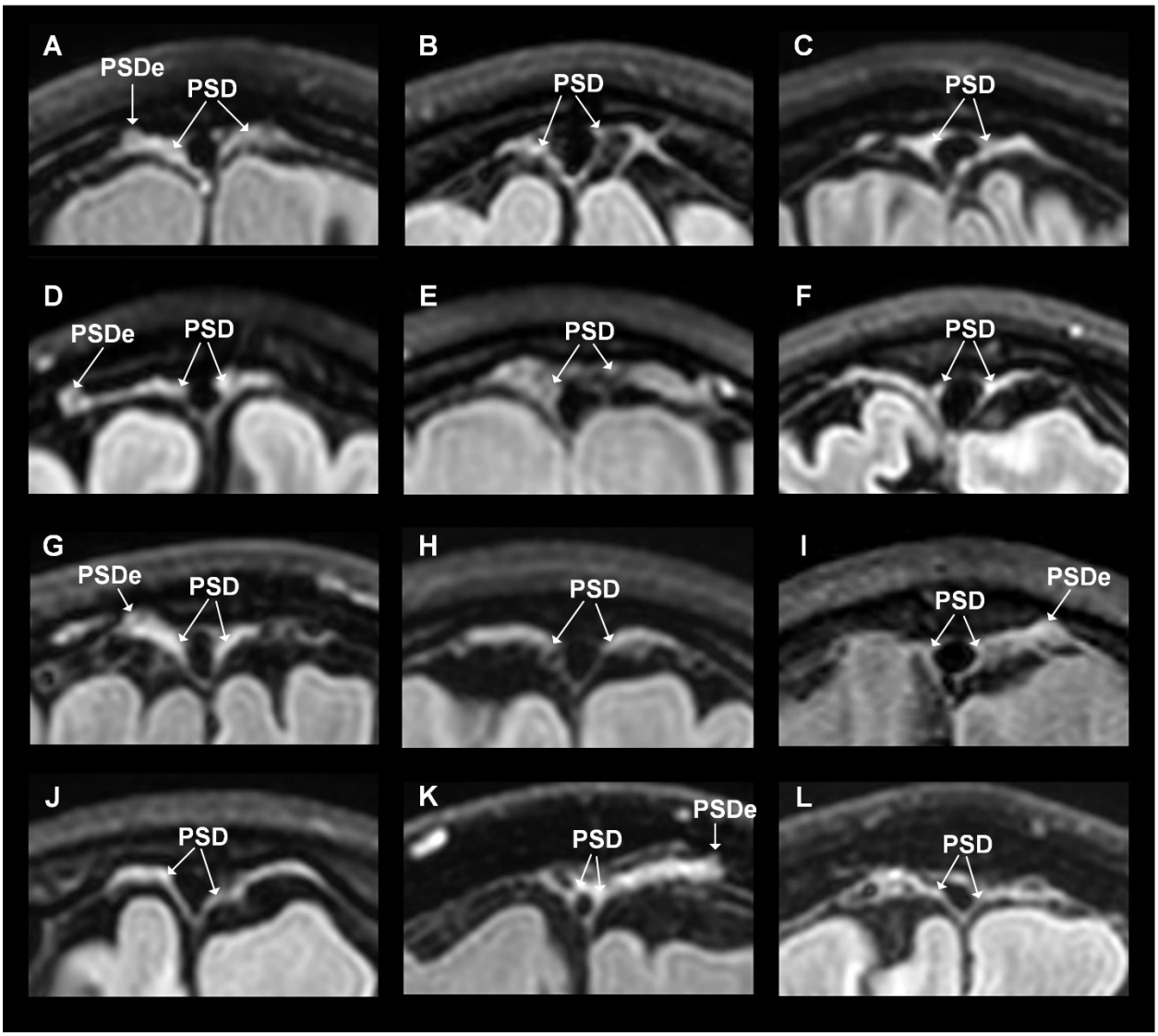

Suppl. Fig 5. Examples of variation in size of parasagittal dura (coronal sections at skull vertex). Examples from T2-FLAIR images demonstrate anatomical variety in parasagittal dura (PSD) volume and configuration: (**A**) Reference subject, 44 years. (**B**) Reference subject, 25 years. (**C**) Reference subject, 26 years. (**D**) Individual with arachnoid cyst, 32 years. (**E**) Reference subject, 28 years. (**F**) Individual with spontaneous intracranial hypotension, 34 years. (**G**) Individual with arachnoid cyst, 48 years. (**H**) Individual with arachnoid cyst, 30 years. (**I**) Individual with arachnoid cyst, 58 years. (**J**) Individual with arachnoid cyst, 20 years. (**K**) Individual with idiopathic intracranial hypertension, 57 years. (**L**) Individual with spontaneous intracranial hypotension, 52 years. PSD and parasagittal dura extensions (PSDe) are indicated by arrows.

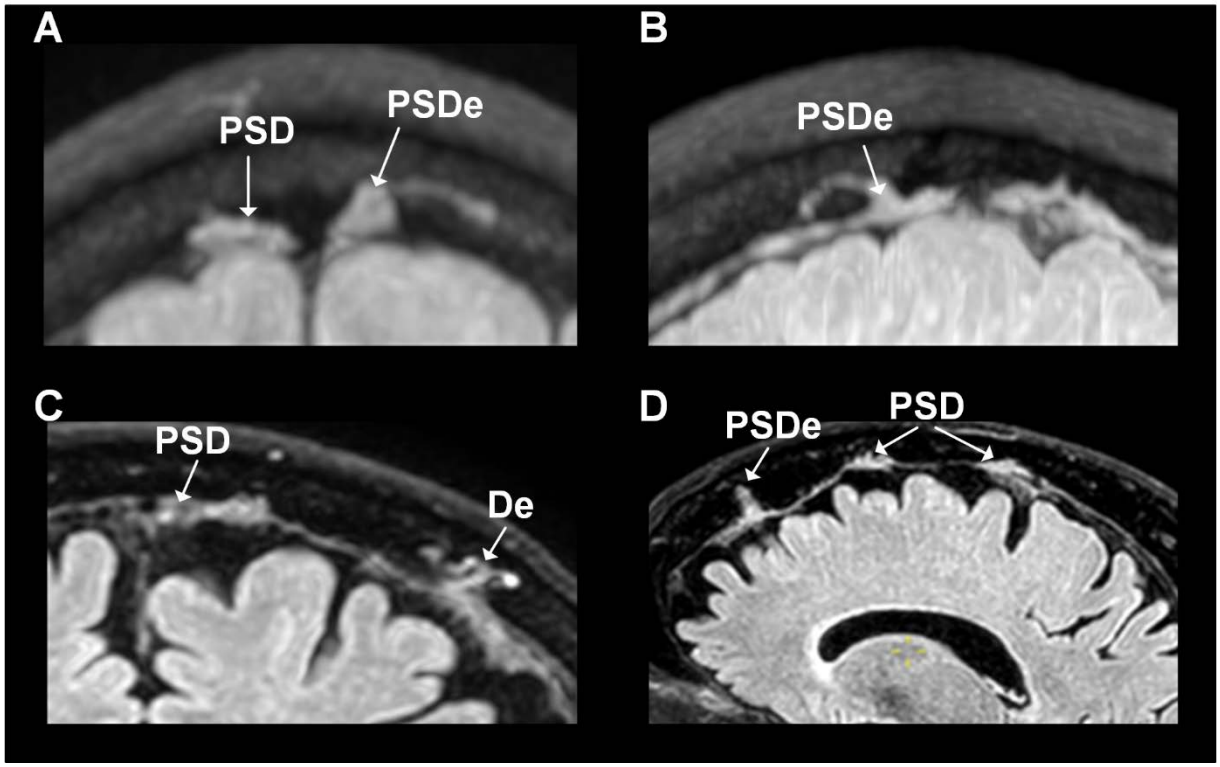

Suppl. Fig. 6. Illustrations of morphological characteristics of parasagittal dura (PSD) and extensions of parasagittal dura (PSDe) into diploe of skull bone marrow (FLAIR imaging). A 55-year-old individual with idiopathic intracranial hypertension (IIH) presenting with voluminous PSD and PSDe presented in (**A**) coronal and (**B**) sagittal, 10 mm thick sections. PSD does not extend through the inner table of the skull, whereas PSDe does. A 71-year-old patient with idiopathic normal pressure hydrocephalus (iNPH) with prominent PSD and dural extensions (De) into diploic areas in distance from PSD presented in (**C**) coronal and (**D**) sagittal, 1 mm thick sections.

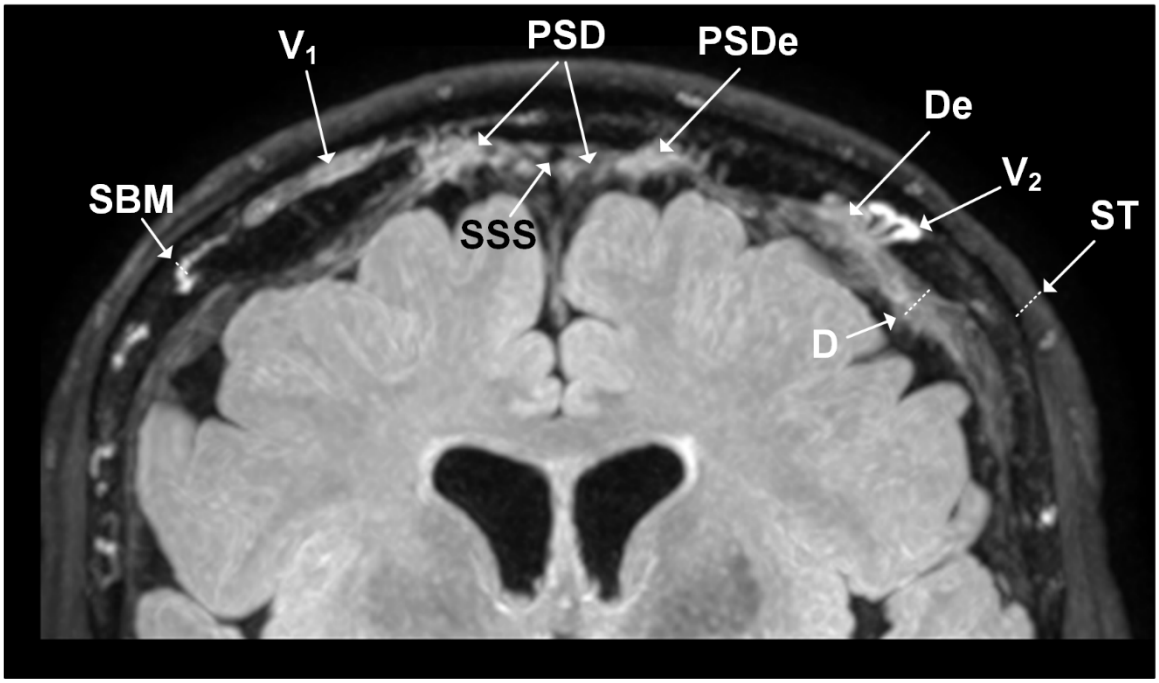

Suppl. Fig. 7. Examples of dural extensions into diploic area visualized by thick MRI (FLAIR), coronal section. Variability of dural extensions into skull bone marrow (SBM) with prominence in the upper extreme of the study cohort is illustrated by a 20 mm thick slab of MRI T2-FLAIR. D: Dura. De: Dura extensions to diploe in distance from parasagittal dura. PSD: Parasagittal dura. PSDe: Dura extensions to diploe from parasagittal dura. SBM: Skull bone marrow. SSS: Superior sagittal sinus. ST: Superficial soft tissue. V1 and V2: Intradiploic veins.

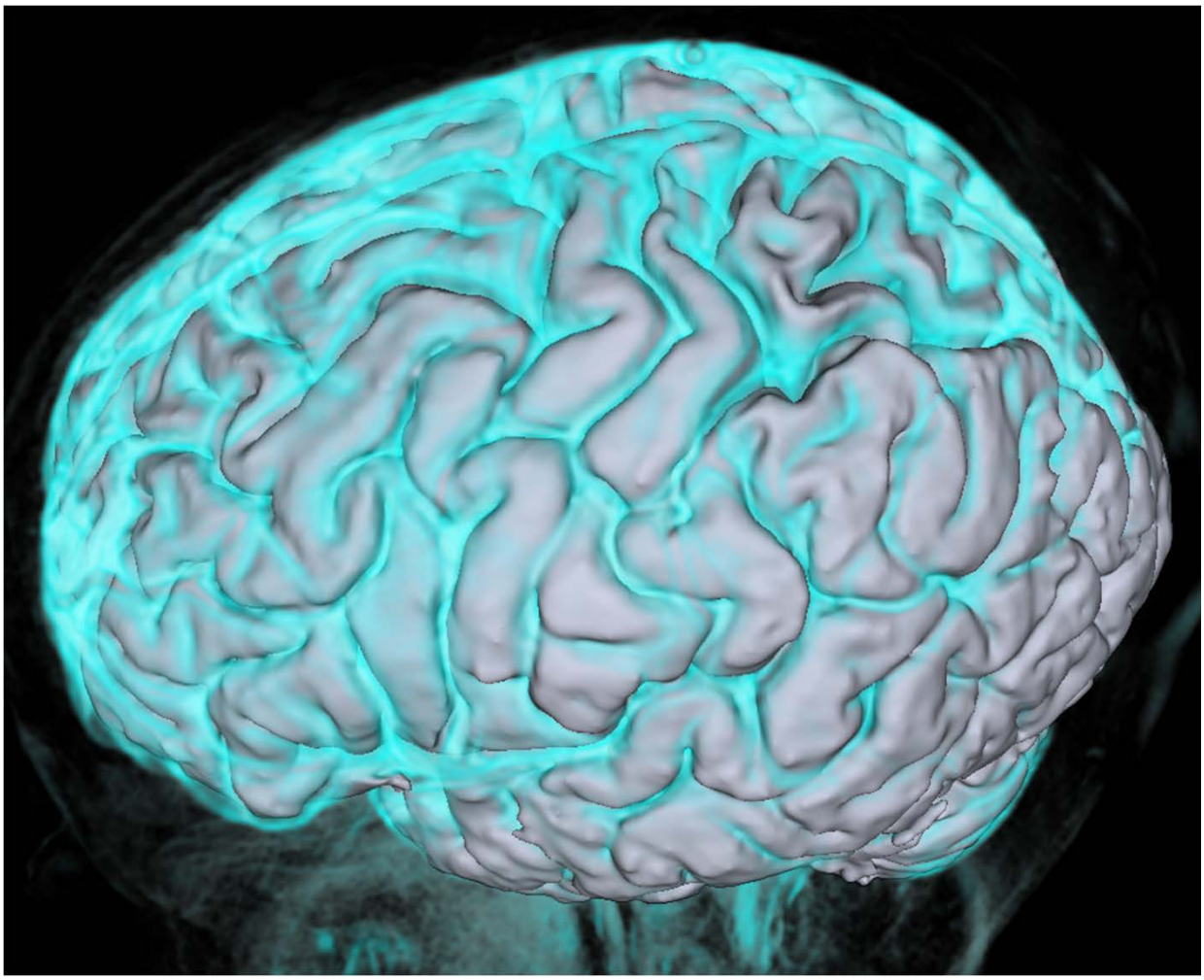

Suppl. Fig. 8. Intrathecal injection of tracer enriches cerebrospinal fluid (CSF) of subarachnoid space at the brain convexities (upper lateral view). The tracer (turquoise) had distributed within CSF of subarachnoid space around the entire cortical surface 24 hours after administration. Among the 53 individuals included in the study, the time from intrathecal injection of tracer until first appearance in cisterna magna (spinal transit time) was 25.3 ± 48.1 minutes. The magnitude of tracer enrichment within parasagittal dura extensions (PSDe) correlated strongly with the availability of tracer in nearby CSF (Suppl Fig. 10); likewise tracer enrichment in dural extensions (De) in distance from parasagittal dura showed the same correlation pattern (Suppl. Fig 11). Image: Tomas Sakinis, MD

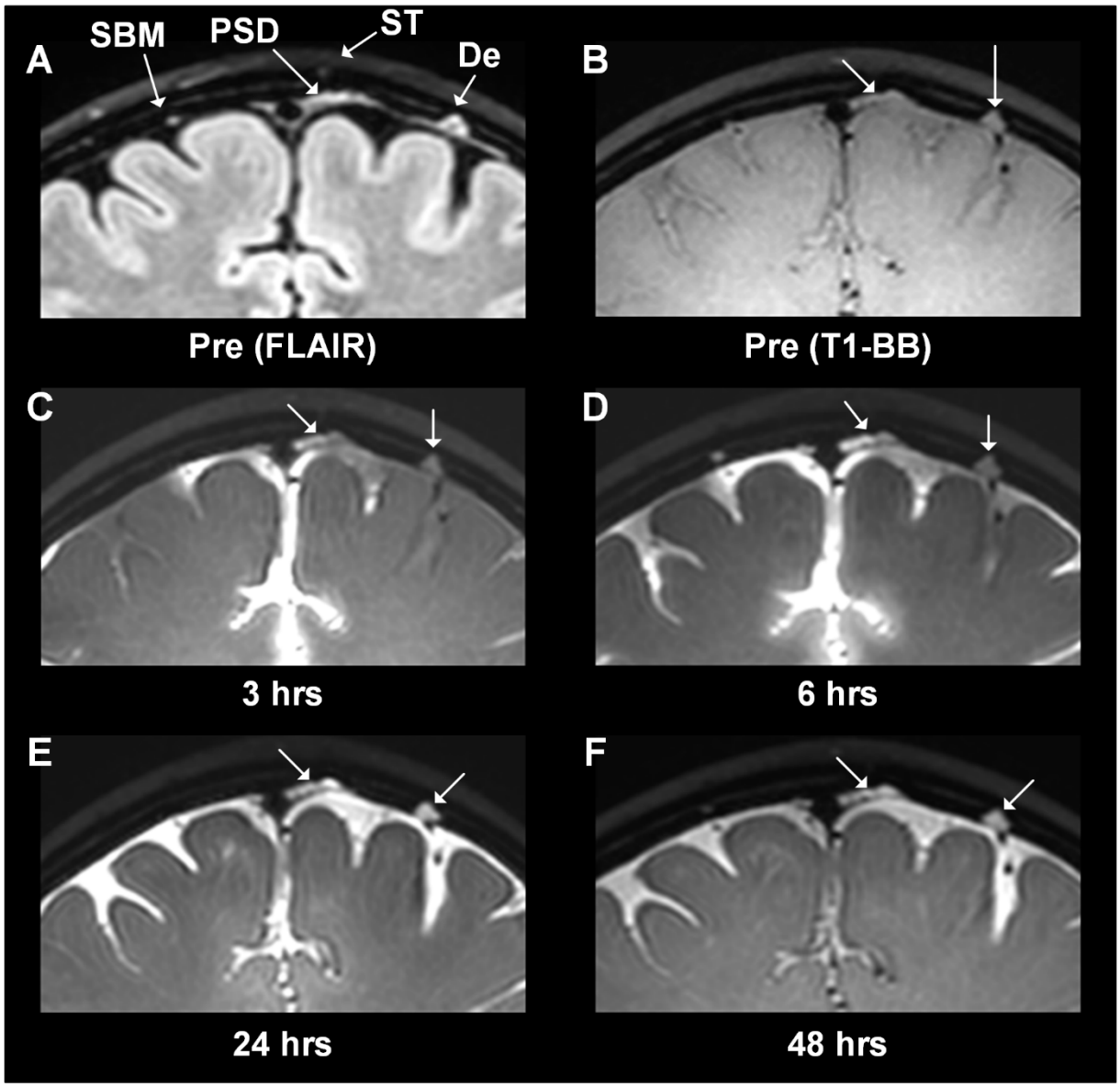

Suppl Fig. 9. Tracer enrichment in parasagittal dura and a dural extension into diploe of skull bone marrow over time. (**A**) The coronal T2-FLAIR MR image shows a typical feature of extra-diploic parasagittal dura (PSD) with high signal, and a dural extension (De) into diploe of skull bone marrow (SBM) in distance from PSD. ST: Superficial tissue. (**B**) The same structures are shown in a pre-contrast T1-BB image. The changes in signal intensity within PSD and De from before tracer injection (Pre) are indicated and after (**C**) 3 h, (**D**) 6 h, (**E**) 24 h and (**F**) 48 h. For this 32 years individual under work-up for an arachnoid cyst, the percentage normalized T1-BB signal unit increase was: (B; Pre. PSD: 1.87. De: 1.59), (C, 3h. PSD: 2.15. De: 1.95), (D, 6h. PSD: 6.49. De: 3.08), (D, 24h. PSD: 5.98. De: 5.44), and (F, 48h. PSD: 3.86. De: 5.80). Signal increase within the subarachnoid space at the brain surface (c-f) is from tracer (gadobutrol) enrichment within CSF.

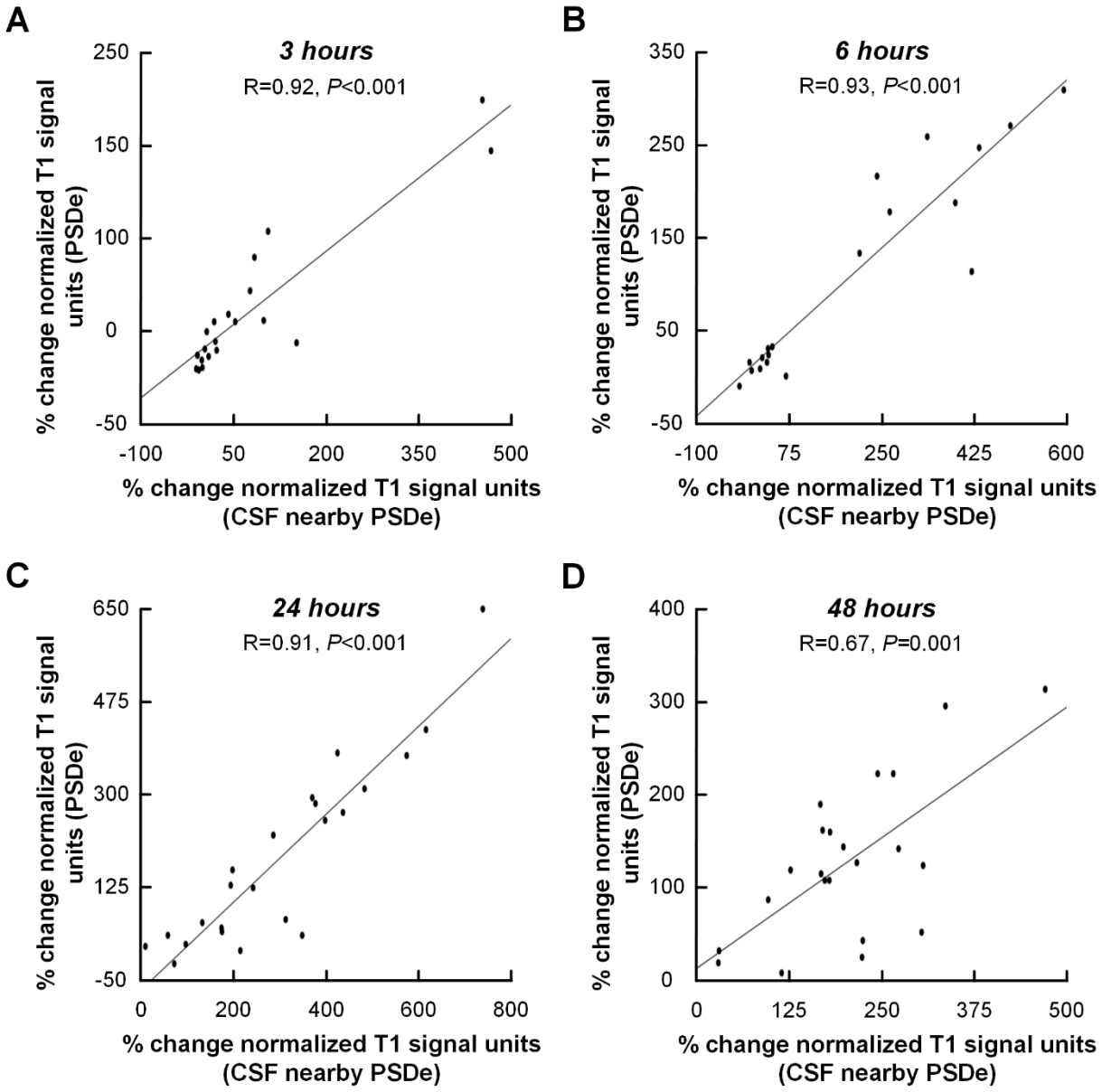

Suppl. Fig. 10. Correlations between tracer enrichment in dura extensions from parasagittal dura and within CSF space. There was a highly significant positive correlation between tracer enrichment in intradiploic dura extensions from parasagittal dura (PSDe) and within nearby CSF spaces at (**A**) 3 h, (**B**) 6 h (**C**) 24 h, (**D**) and 48 h. Each plot presents the fit line and the Pearson correlation coefficient (R) with P-value. PSDe: Dura extensions to diploe from parasagittal dura.

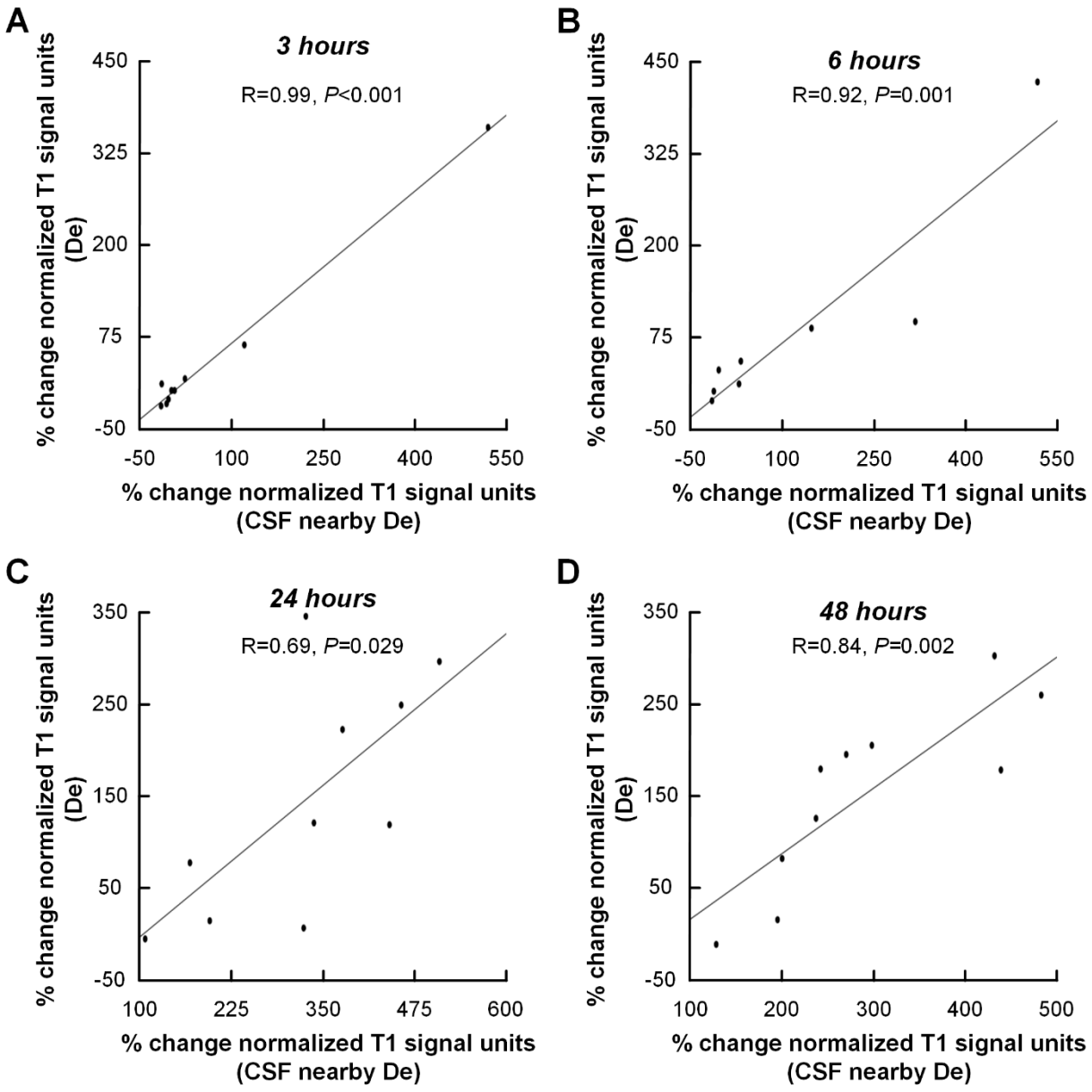

Suppl. Fig. 11. Correlations between tracer enrichment within dura extensions to diploic skull space and within CSF over time. There was a highly significant positive correlation between tracer enrichment in dural extensions (De) and within nearby CSF spaces at (**A**) 3 h, (**B**) 6 h, (**C**) 24 h and (**D**) 48 h. Each plot presents the fit line and the Pearson correlation coefficient (R) with P-value. De: Dura extensions to diploe in distance from parasagittal dura.

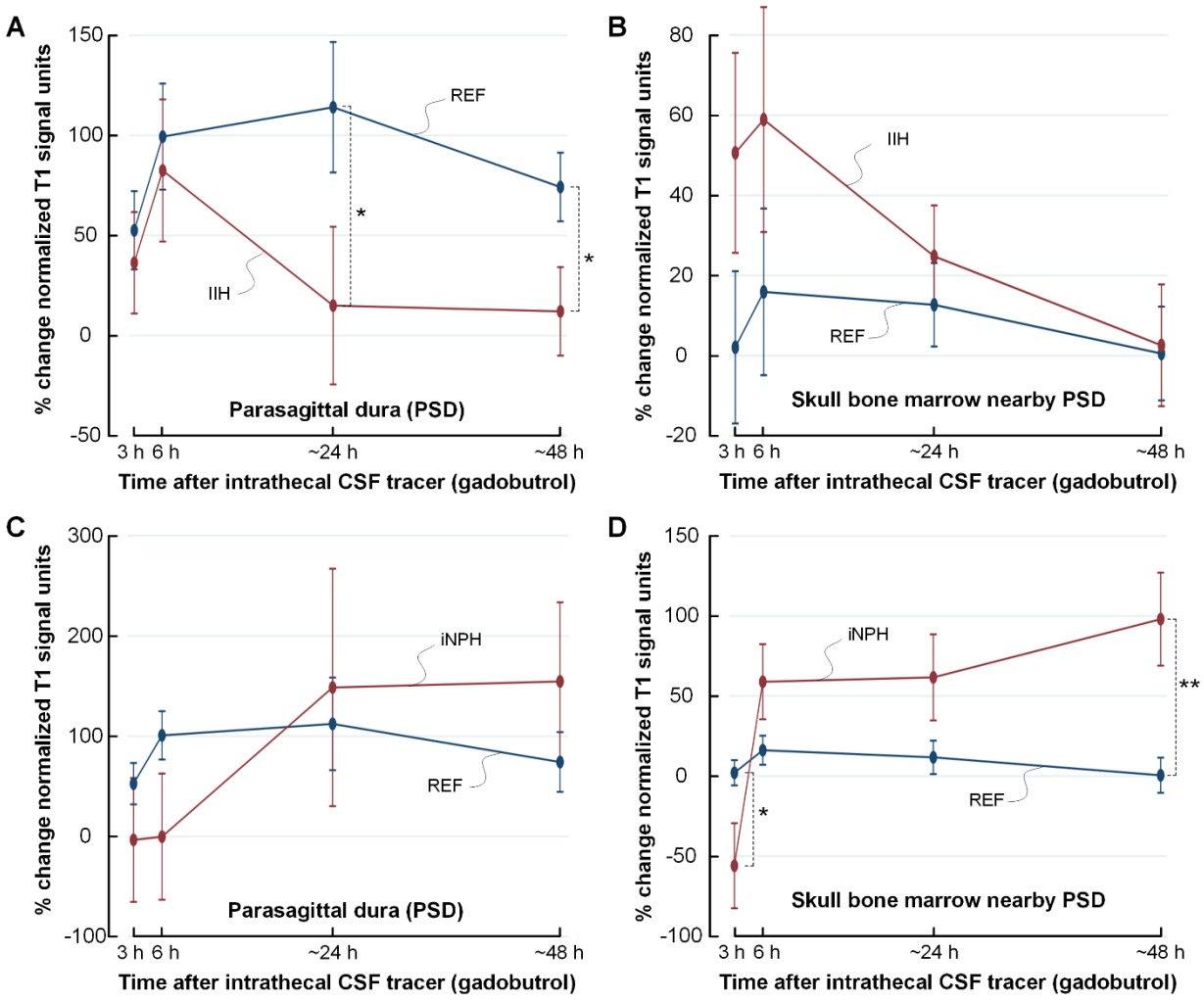

Suppl. Fig. 12. Tracer enrichment over time in parasagittal dura and skull bone marrow depending on underlying brain pathology. The trend plots of percentage change in tracer (gadobutrol) enrichment (normalized T1-BB signal unit ratio) within parasagittal dura (PSD) and skull bone marrow of reference patients (n=14), and compared with patients with (**A**-**B**) IIH (n=10), and (**C**-**D**) iNPH (n=2). Trend plots are presented with mean ± standard error (SE). Statistical differences: *P<0.05, **P<0.01, ***P<0.001 (linear mixed models).

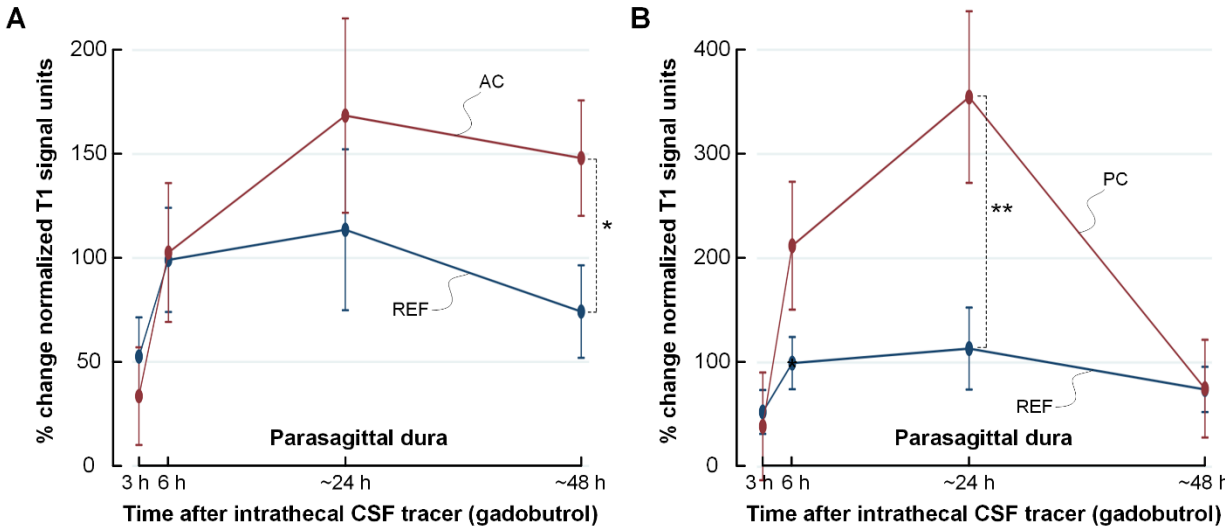

Suppl. Fig. 13. Trend plots of tracer enrichment within parasagittal dura of reference patients and patients with intracranial cysts. The trend plots of percentage change in tracer enrichment (normalized signal unit ratio) within parasagittal dura of reference (REF) patients (n=14), and compared with patients with (**A**) arachnoid cyst (AC; n=3) and (**B**) pineal cyst (PC; n=3). Trend plots are presented with mean ± standard error (SE). Statistical differences: *P<0.05, **P<0.01, ***P<0.001 (linear mixed models).

Suppl. Table 1. Percentage change in normalized T1-BB signal units over time for different patient

Patient Groups	Parasagittal dura (PSD)				Skull bone nearby parasagittal dura (PSD)			
	3 hrs	**6 hrs**	**24 hrs**	**48 hrs**	**3 hrs**	**6 hrs**	**24 hrs**	**48 hrs**
REF	53 ± 21[a]	101 ± 24[c]	112 ± 46[a]	74 ± 30[a]	2 ± 8	16 ± 9	12 ± 10	1 ± 11
iNPH	-4 ± 62	0 ± 63	149 ± 119	155 ± 79[a]	-56 ± 27[a]	59 ± 24[a]	62 ± 27[a]	98 ± 29[b]
Diff (REF – iNPH)	-56 ± 65	-101 ± 67	36 ± 127	80 ± 84	-58 ± 28[a]	43 ± 25	50 ± 29	98 ± 31[b]
REF	53 ± 20[a]	101 ± 23[c]	112 ± 44[a]	74 ± 27[b]	2 ± 11	16 ± 12	11 ± 12	1 ± 13
cHC	3 ± 54	-6 ± 60	44 ± 113	108 ± 70	70 ± 28[a]	58 ± 30[a]	88 ± 31[b]	87 ± 34[a]
Diff (REF – cHC)	-49 ± 58	-107 ± 65	-68 ± 121	34 ± 75	68 ± 30[a]	42 ± 32	77 ± 34[a]	86 ± 37[a]
REF	53 ± 20[b]	100 ± 24[c]	113 ± 42[b]	74 ± 27[b]	2 ± 8	16 ± 9	12 ± 9	1 ± 10
SIH	36 ± 34	88 ± 40[a]	199 ± 69[b]	128 ± 44[b]	18 ± 14	10 ± 15	4 ± 15	3 ± 17
Diff (REF – SIH)	-17 ± 39	-12 ± 46	87 ± 81	54 ± 52	16 ± 17	-6 ± 18	-8 ± 18	2 ± 20
REF	53 ± 20[b]	99 ± 27[c]	114 ± 33[c]	74 ± 17[c]	2 ± 19	16 ± 21	13 ± 10	1 ± 12
IIH	36 ± 25	83 ± 36[a]	15 ± 39	12 ± 22	51 ± 25[a]	59 ± 28[a]	25 ± 13[a]	3 ± 15
Diff (REF – IIH)	-16 ± 32	-17 ± 44	-99 ± 51[a]	-62 ± 28[a]	49 ± 31	43 ± 35	12 ± 16	2 ± 19
REF	53 ± 19[b]	99 ± 25[c]	114 ± 39[b]	74 ± 22[b]	2 ± 8	16 ± 10	12 ± 11	1 ± 10
AC	34 ± 24	103 ± 33[b]	169 ± 47[c]	148 ± 28[c]	40 ± 10[c]	5 ± 14	16 ± 13	12 ± 12
Diff (REF – AC)	-19 ± 30	4 ± 42	55 ± 61	74 ± 36[a]	38 ± 13[b]	-11 ± 17	4 ± 17	11 ± 16
REF	53 ± 21[a]	100 ± 25[c]	113 ± 39[b]	74 ± 22[b]	2 ± 8	16 ± 9	12 ± 9	1 ± 10
PC	39 ± 52	212 ± 61[b]	355 ± 82[c]	75 ± 47	23 ± 19	-7 ± 22	25 ± 20	-16 ± 21
Diff (REF – PC)	-14 ± 56	113 ± 66	241 ± 91[b]	1 ± 52	21 ± 20	-24 ± 23	14 ± 22	-17 ± 24

AC: Arachnoid cyst. cHC: Communicating hydrocephalus. IIH: Idiopathic intracranial hypertension. iNPH: Idiopathic normal pressure hydrocephalus. PC: Pineal cyst. REF: SIH: Spontaneous intracranial hypotension. The signal change, indicative of tracer enrichment, was highly significant for several locations (linear mixed model analysis; *P<0.05, **P<0.01, ***P<0.001), with peak at 24 h. Trend plots presented by mean and error bars as standard errors.